Available online at www.sciencedirect.com
ScienceDirect
Mechatronics 17 (2007) 15–30
MECHATRONICS

Current sensorless position–flux tracking controller for induction motor drives ☆

Marcello Montanari [a], Sergei Peresada [b], Carlo Rossi [a], Andrea Tilli [a,*]

[a] Center for Research on Complex Automated Systems "G. Evangelisti" (CASY), Department of Electronics, Computer Science and Systems (DEIS), University of Bologna, Viale Risorgimento 2, 40136 Bologna, Italy

[b] Department of Electrical Engineering, National Technical University of Ukraine "Kiev Polytechnic Institute", Prospect Pobedy 37, Kiev 252056, Ukraine

Received 27 July 2005; accepted 6 July 2006

Abstract

An innovative indirect field-oriented output feedback controller for induction motor drives is presented. This solution is based on output feedback since only speed and position of the motor shaft are measured, while current sensors are avoided. This approach is suitable for low cost applications, where the position sensor cannot be removed to guarantee accurate position tracking.

The proposed method provides global asymptotic tracking of smooth position and flux references in presence of unknown constant load torque. It is based on the natural passivity of the electromagnetic part of the machine and it guarantees asymptotic decoupling of the induction motor mechanical and electrical subsystems achieving at the same time asymptotic field orientation. Lyapunov analysis and nonlinear control design have been adopted to obtain good position tracking performances and effective torque–flux decoupling. The cascaded structure of the controller allows performing a constructive tuning procedure for speed and position control loops.

Results of experimental tests are presented to demonstrate the tracking and robustness features of the proposed solution.
© 2006 Elsevier Ltd. All rights reserved.

Keywords: Induction motors; Position control; Speed control; Cascade control; Lyapunov methods

1. Introduction

In the last decades vector-controlled AC drives, based on different kind of AC motors, have become the most spread electromechanical systems to generate controlled motion with high accuracy and high dynamic requirements [1,2].

The most common AC motor used in servo applications is the Permanent Magnet Synchronous Motor (PMSM), owing to its small dimensions and the high dynamic performance achievable thanks to its large torque/inertia ratio. Induction Motor (IM) vector drives are usually adopted when the required dynamic performances are not extreme, weight and spaces are not crucial or when the required power cannot be handled by a PMSM.

Different control strategies have been proposed to solve the speed/position and flux control problem for IM. An extensive overview is presented in [3]. The most relevant theoretical results, starting from the pioneering work of Blaschke [4], are presented in [5], where feedback linearization was exploited; in [6,7] where passivity approach is adopted; in [8,9] where back-stepping design procedure is used; and [10] where high gain technique is applied. Two advanced speed/flux tracking IM controllers, based on Indirect Field Oriented Control (IFOC), are considered in [11,6]. The first is based on Improved Indirect Field Orientation (I-IFO), leading to general decomposition of the resulting speed–flux error dynamics into electromechanical and electromagnetic subsystems, while the second exploits

☆ This paper has not been previously presented at any conference.

* Corresponding author. Tel.: +39 051 2093924; fax: +39 051 2093073.
E-mail addresses: mmontanari@deis.unibo.it (M. Montanari), peresada@i.com.ua (S. Peresada), crossi@deis.unibo.it (C. Rossi), atilli@deis.unibo.it (A. Tilli).

0957-4158/$ - see front matter © 2006 Elsevier Ltd. All rights reserved.
doi:10.1016/j.mechatronics.2006.07.001

general decomposition into interconnected mechanical and electrical dynamics. In [12] it is shown that I-IFO control demonstrates not only higher dynamic performance as compared with standard IFOC, but also relevant robustness properties with respect to rotor circuit parameters variation.

All the above-mentioned algorithms, which give excellent performance, are based on stator currents and rotor speed/position measurements. Nevertheless, for a wide range of low power, medium performance applications, where high dynamic performance is not needed, but quite good accuracy of position regulation/tracking is required, both PMSM and IM standard vector drives are quite expensive.

DC-brushless drives are often used to cope with such applications profitably, but some drawbacks are actually present. Hall-effect sensors have to be embedded in the DC-brushless motor to detect the position of the rotor permanent magnet. For quite accurate servo tasks where encoder or resolver sensors are adopted, Hall-effect sensors can be avoided for phase current commutations, nevertheless estimation of the initial position of the permanent magnet and rotor alignment must be performed. Anyhow, the most relevant drawback of DC-brushless motors with trapezoidal field is the torque ripple, which is due to magnetic field anisotropy (for the presence of permanent magnet and variable reluctance) and phase current commutations. This negative feature is not so relevant for low-accuracy positioning, but could be crucial when good positioning or low-speed control are required and it can be compensated only using involved control algorithms, leading to relevant rise of drive cost.

Hence, low cost position/speed controlled IM drives could be an attractive alternative for such applications since IMs have a negligible torque ripple. Moreover, this kind of drives covers a wider range of power sizes with respect to DC-brushless. Actually, drives based on V/f control [1] and standard inverter-duty IM are already adopted with an additional speed/position control loop based on encoder/resolver sensors. For this kind of solution no current sensor is adopted to measure the phase currents of the motor and low cost, low performance microprocessors can be used to control the drive, thus reducing costs with respect to standard vector drives. On the other hand, this approach gives very poor speed/position control dynamic performances [13], since:

- no speed/position tracking can be obtained, i.e. only accurate positioning is guaranteed;
- torque delivered by the motor cannot be controlled directly;
- sudden load torque variations lead to relevant oscillatory transients.

According to the above considerations, the main aim of this work is to present a novel position control for IM with the following features:

- hardware and software requirements fitting the case of standard V/f drives adopted for position control, i.e. utilization of the position/speed sensor, absence of current sensors and low computational burden and sampling rate;
- good dynamic performance allowing tracking of variable position/speed and flux trajectories;
- good load torque rejection.

From a control viewpoint the proposed solution differs from standard vector control owing to the absence of stator current measurements, hence it can be classified as ''current sensorless'' or ''output feedback''. It is worth to point out that ''sensorless control'' is commonly adopted to identify solutions where no position/speed sensor is used. On the other hand, this work focuses on positioning applications, such as pick and place and cutting machines, where the rotor shaft position/speed sensor cannot be removed to guarantee accuracy and reliability. Hence, no correlation is present between the proposed ''current sensorless'' solution and the common ''sensorless control''.

Current sensorless control of IM has been already considered in previous works [13–16], where Indirect Field-Orientation concept has been exploited without a deep theoretical analysis. Tracking of variable position and flux trajectories have not been considered in these papers. In [17], a current sensorless speed–flux tracking control is reported. An adaptation mechanism is added to estimate the parameters of the IM mechanical part. This solution, developed in the stationary reference frame, is complex even removing the adaptation mechanism. In [18] the motivations and design concepts for the development of a low cost inverter for IM are considered.

In this paper a new indirect field-oriented output feedback controller for induction motor drives, which provides global asymptotic tracking of smooth position and flux references in presence of unknown constant load torque, is presented. The solution is based on the natural passivity of the electromagnetic part of the machine and guarantees asymptotic decoupling of the induction motor mechanical and electrical subsystems achieving at the same time asymptotic field orientation. Lyapunov analysis and nonlinear control design have been adopted to obtain good position tracking and effective torque–flux decoupling, leading to performances very close to standard IM vector drives with current sensors and current feedback control.

It is worth noting that the IFOC is intrinsically open-loop with respect to magnetic flux regulation, hence both the solutions reported in [15] and the one proposed in this paper extend this kind of approach to stator current control by means of suitable feed-forward actions. Despite their ''full open-loop nature'' with respect to the electromagnetic part, the above-mentioned algorithms guarantee good robustness in terms of position/speed tracking and field orientation. A physical explanation of such result is reported in [15].

The computational load of the presented approach is slightly larger than the V/f one, but the sampling frequency

required for digital implementation can be significantly smaller than the vector control one, owing to the elimination of the current feedback control. Moreover, in the V/f position control algorithm the controller tuning rules are obscure, owing to the heuristic nature of such solution, while for the proposed algorithm they are clear, thanks to the decoupling between mechanical and electromagnetic parts.

The novelty of this paper is that a new current sensorless IM controller for position–flux tracking with solid theoretical background and clear and simple structure, based on natural passivity properties of the IM, is presented. With respect to other solutions such as the "V-type" control in [15], it guarantees better dynamic performance with comparable complexity.

The paper is organized as follows. In Section 2, the IM model is reported and the control problem is formulated, recalling the IFO concept. The control design is described in Section 3. The current/flux subsystem design based on rigorous Lyapunov analysis is reported in Section 3.1, while the position/speed controller design is reported in Section 3.2; particular attention is devoted to the analysis of the overall system stability properties. In Section 4, the proposed solution is compared with the so-called "V-type" control presented in [15]. The aim is to highlight how the proposed algorithm guarantees better torque–flux decoupling and, consequently, better control performances. In Section 5, experimental results are shown to demonstrate tracking capability and robustness with respect to parameter variations of the solution proposed.

2. Induction motor model and control problem statement

2.1. Induction motor model

The equivalent two-phase model of symmetrical IM, under assumptions of linear magnetic circuits and balanced operating conditions, is presented in an arbitrary rotating reference frame (d–q) [1] as

$$\begin{aligned}
\dot{\theta} &= \omega,\\
\dot{\omega} &= \mu(\psi_d i_q - \psi_q i_d) - \frac{T_L}{J} - v\omega,\\
\dot{i}_d &= -\gamma i_d + \omega_0 i_q + \alpha\beta\psi_d + \beta\omega\psi_q + \frac{1}{\sigma}u_d,\\
\dot{i}_q &= -\gamma i_q - \omega_0 i_d + \alpha\beta\psi_q - \beta\omega\psi_d + \frac{1}{\sigma}u_q,\\
\dot{\psi}_d &= -\alpha\psi_d + (\omega_0 - \omega)\psi_q + \alpha L_m i_d,\\
\dot{\psi}_q &= -\alpha\psi_q - (\omega_0 - \omega)\psi_d + \alpha L_m i_q,\\
\dot{\varepsilon}_0 &= \omega_0,
\end{aligned} \tag{1}$$

where $\mathbf{i} = (i_d, i_q)^T$, $\mathbf{\Psi} = (\psi_d, \psi_q)^T$, $\mathbf{u} = (u_d, u_q)^T$ denote stator current, rotor flux and stator voltage vectors. Subscripts d and q stand for vector components in the (d–q) reference frame, θ, ω are the rotor position and speed, T_L is the load torque and ε_0, ω_0 are the angular position and speed of the (d–q) reference frame with respect to the fixed stator reference frame (a–b), where the physical variables are defined. Transformed variables in (1) are given by

$$\begin{aligned}
\mathbf{x}_{dq} &= e^{-j\varepsilon_0}\mathbf{x}_{ab}\\
\mathbf{x}_{ab} &= e^{j\varepsilon_0}\mathbf{x}_{dq}
\end{aligned} \quad \text{where } e^{j\varepsilon_0} = \begin{bmatrix} \cos\varepsilon_0 & -\sin\varepsilon_0 \\ \sin\varepsilon_0 & \cos\varepsilon_0 \end{bmatrix}, \tag{2}$$

where $\mathbf{x}_{yz}$ stands for any two-dimensional vectors of IM.

Positive constants related to the electrical and mechanical parameters of the IM are defined as follows:

$$\sigma = L_s\left(1 - \frac{L_m^2}{L_s L_r}\right), \quad \beta = \frac{L_m}{\sigma L_r}, \quad \mu = \frac{3}{2}\frac{L_m}{JL_r}, \quad \alpha = \frac{R_r}{L_r},$$
$$\gamma = \frac{R_s}{\sigma} + \alpha L_m \beta,$$

where J is the total rotor inertia, v is the friction coefficient, R_s, R_r, L_s, L_r are stator/rotor resistances and inductances respectively, L_m is the magnetizing inductance. One pole pair is assumed without loss of generality.

2.2. Control objectives

General specification for position-controlled electric drives requires to control the two IM outputs, position and rotor flux modulus, defined as

$$\mathbf{y}_1 = \begin{bmatrix} \theta \\ (\psi_d^2 + \psi_q^2)^{1/2} \end{bmatrix} \triangleq \begin{pmatrix} \theta \\ |\psi| \end{pmatrix} \tag{3}$$

using the two-dimensional stator voltage vector $\mathbf{u}$ on the basis of measured variables vector $\mathbf{y} = (\theta, \omega)^T$.

Define $\mathbf{y}_1^* = (\theta^*, \psi^*)^T$, where θ^* and $\psi^* > 0$ are position and flux reference trajectories. The position and flux modulus tracking errors are

$$\begin{aligned}
\tilde{\theta} &= \theta - \theta^*,\\
\tilde{\psi} &= |\psi| - \psi^*.
\end{aligned} \tag{4}$$

Following IFO concepts [11], the d and q axis flux tracking errors are defined as

$$\begin{aligned}
\tilde{\psi}_d &= \psi_d - \psi^*,\\
\tilde{\psi}_q &= \psi_q.
\end{aligned} \tag{5}$$

Note that $\lim_{t\to\infty}\tilde{\psi}_q = 0$ is the condition of asymptotic field orientation. From (4) and (5) it follows that condition $\lim_{t\to\infty}(\tilde{\psi}_d, \tilde{\psi}_q) = 0$ implies $\lim_{t\to\infty}\tilde{\psi} = 0$.

The position–flux tracking problem is formulated as follows. Consider the IM model (1) and (2) and assume that:

- A.1. Rotor position and speed are available from measurements.
- A.2. Motor parameters are known and constant.
- A.3. Load torque T_L is unknown but constant and bounded.
- A.4. Position and flux reference trajectories θ^*, $\psi^* > 0$ are smooth functions with known and bounded $\dot{\theta}^*$, $\ddot{\theta}^*$, θ^*, $\dot{\psi}^*$, $\ddot{\psi}^*$.

Under these assumptions, it is required to design an output feedback controller satisfying the following control objectives:

CO1. Global asymptotic position–flux tracking and asymptotic field orientation, i.e.

$$\lim_{t\to\infty}\tilde{\theta}=0,\quad \lim_{t\to\infty}\tilde{\psi}_d=0,\quad \lim_{t\to\infty}\tilde{\psi}_q=0, \tag{6}$$

with all signals bounded.

CO2. Asymptotic decoupling of the output variables, namely, if $\tilde{\psi}_d(0)=0$, $\tilde{\psi}_q(0)=0$, then $\tilde{\psi}_d(t)=\tilde{\psi}_q(t)\equiv 0$, $\forall t\geqslant 0$ and the dynamics of the mechanical error variables is independent of the flux control.

CO3. Linear dynamics of the nominal (i.e. with $\tilde{\psi}_d=\tilde{\psi}_q=0$) speed/position subsystem.

3. Controller design

The flux–current subsystem is designed first, in order to satisfy the flux–current tracking control objective achieving at the same time asymptotic field orientation. Then, the mechanical subsystem is designed to ensure the speed–position tracking.

3.1. Current–flux subsystem design

The objectives of the flux–current controller are:

- to generate the flux vector angle reference trajectory $\varepsilon_0(t)$;
- to guarantee globally exponentially stable flux–current (torque) tracking by means of a suitably designed control voltage vector $(u_d,u_q)^{\mathrm{T}}$.

Define the stator current references i_d^*, i_q^* and the corresponding current tracking errors

$$\tilde{i}_d=i_d-i_d^*,\quad \tilde{i}_q=i_q-i_q^*. \tag{7}$$

The following control algorithm is adopted for the IM electrical subsystem:

- Flux controller

$$\begin{aligned} i_d^* &= \frac{1}{\alpha L_{\mathrm{m}}}(\alpha\psi^*+\dot{\psi}^*),\\ \dot{\varepsilon}_0 &= \omega_0=\omega+\alpha L_{\mathrm{m}}\frac{i_q^*}{\psi^*}. \end{aligned} \tag{8}$$

- Current controller

$$\begin{aligned} u_d &= \sigma(\gamma i_d^*-\omega_0 i_q^*-\alpha\beta\psi^*+\dot{i}_d^*),\\ u_q &= \sigma(\gamma i_q^*+\omega_0 i_d^*+\beta\omega\psi^*+\dot{i}_q^*). \end{aligned} \tag{9}$$

Substituting the flux–current control algorithm into (1) the error dynamics of the IM electrical subsystem becomes

$$\dot{\mathbf{x}}_{\mathrm{e}}=\begin{bmatrix} -\gamma & \omega_0 & \alpha\beta & \beta\omega\\ -\omega_0 & -\gamma & -\beta\omega & \alpha\beta\\ \alpha L_{\mathrm{m}} & 0 & -\alpha & \omega_2\\ 0 & \alpha L_{\mathrm{m}} & -\omega_2 & -\alpha \end{bmatrix}\mathbf{x}_{\mathrm{e}}\triangleq\mathbf{A}_{\mathrm{e}}(t)\mathbf{x}_{\mathrm{e}}, \tag{10}$$

where $\mathbf{x}_{\mathrm{e}}=(\tilde{i}_d,\tilde{i}_q,\tilde{\psi}_d,\tilde{\psi}_q)^{\mathrm{T}}$, $\omega_2=\omega_0-\omega$ is the slip angular frequency and signals ω_0, ω, ω_2 in $A_{\mathrm{e}}(t)$ are considered as bounded external inputs in the following preliminary analysis.

In order to investigate the stability properties of the non-autonomous linear system (10), consider the following Lyapunov function:

$$V=\frac{1}{2}\mathbf{x}_{\mathrm{e}}^{\mathrm{T}}\mathbf{P}\mathbf{x}_{\mathrm{e}}, \tag{11}$$

with

$$\mathbf{P}=\begin{bmatrix} \frac{\varepsilon}{\beta} & 0 & \varepsilon & 0\\ 0 & \frac{\varepsilon}{\beta} & 0 & \varepsilon\\ \varepsilon & 0 & 1 & 0\\ 0 & \varepsilon & 0 & 1 \end{bmatrix}>0\quad\text{and}\quad \varepsilon<\frac{1}{\beta}. \tag{12}$$

Selecting $\varepsilon=\frac{\alpha L_{\mathrm{m}}}{\gamma}<\frac{1}{\beta}$ and computing the time derivative of V along the trajectories of (10), it holds

$$\dot{V}=-\frac{\varepsilon}{\beta}\frac{R_{\mathrm{s}}}{\sigma}(\tilde{i}_d^2+\tilde{i}_q^2)-\alpha(1-\varepsilon\beta)(\tilde{\psi}_d^2+\tilde{\psi}_q^2)\triangleq-\mathbf{x}_{\mathrm{e}}^{\mathrm{T}}\mathbf{Q}\mathbf{x}_{\mathrm{e}}, \tag{13}$$

hence $\mathbf{P}=\mathbf{P}^{\mathrm{T}}>0$ is solution of the Lyapunov equation $\mathbf{A}_{\mathrm{e}}^{\mathrm{T}}(t)\mathbf{P}+\mathbf{P}\mathbf{A}_{\mathrm{e}}(t)=-\mathbf{Q}$, $\mathbf{Q}=\mathbf{Q}^{\mathrm{T}}>0$.

From (11)–(13) using standard Lyapunov stability arguments it follows that the equilibrium point $\mathbf{x}_{\mathrm{e}}=0$ of system (10) is globally exponentially stable, i.e.

$$\|\mathbf{x}_{\mathrm{e}}(t)\|\leqslant c_1\|\mathbf{x}_{\mathrm{e}}(0)\|\mathrm{e}^{-c_2 t}\quad (c_1,c_2)>0. \tag{14}$$

Asymptotic flux tracking and asymptotic field orientation follow directly from the condition (14), satisfying the second part of CO1. In order to show that torque tracking is achieved as well, consider the IM torque equation

$$T=\frac{3}{2}\frac{L_{\mathrm{m}}}{L_{\mathrm{r}}}\left[\psi^*i_q^*+\psi^*\tilde{i}_q+\tilde{\psi}_d(i_q^*+\tilde{i}_q)-\tilde{\psi}_q(i_d^*+\tilde{i}_d)\right]\triangleq T^*+\tilde{T}, \tag{15}$$

where T^* is the torque reference. Defining in (15)

$$i_q^*=\frac{2}{3}\frac{L_{\mathrm{r}}}{L_{\mathrm{m}}}\frac{T^*}{\psi^*} \tag{16}$$

it follows that

$$\tilde{T}=\frac{3}{2}\frac{L_{\mathrm{m}}}{L_{\mathrm{r}}}[\psi^*\tilde{i}_q+\tilde{\psi}_d(i_q^*+\tilde{i}_q)-\tilde{\psi}_q(i_d^*+\tilde{i}_d)]. \tag{17}$$

For bounded ψ^*, $\dot{\psi}^*$, T^*, current references i_q^* and i_d^* are bounded and therefore $\tilde{T}(t)$ is an exponentially decaying function according to (14), i.e. asymptotic torque tracking is achieved.

Remark 1. The current–flux control algorithm given by (8) and (9) is based on indirect field orientation concept, which is a flux open-loop control strategy according to classical formulation [2]. The proposed flux–current controller is

open-loop with respect to the current control as well. Its stability and robustness properties (see (12) and (13)) are based on the intrinsic stability of the IM electrical part, providing natural indirect field orientation.

Remark 2. The torque reference trajectory has to be bounded with bounded known first time derivative in order to guarantee known first time derivative of the q-axis current reference i_q^*, as required in control algorithm (9).

3.2. Position–speed subsystem design

In this subsection new cascaded position and speed controllers are designed, in order to achieve asymptotic decoupling of mechanical and electrical IM subsystems.

Using (15)–(17) the IM mechanical subsystem in (1) is rewritten as

$$\begin{aligned}\dot\theta &= \omega,\\ \dot\omega &= \mu\psi^* i_q^* - v\omega + \frac{1}{J}(-T_\mathrm{L} + \widetilde T).\end{aligned} \tag{18}$$

Define the speed tracking error as $\tilde\omega = \omega - \omega^*$, where ω^* is the speed reference generated by the position controller, given by

$$\begin{aligned}\omega^* &= \xi_1 + \dot\theta^*,\\ \dot\xi_1 &= -\frac{1}{\tau_1}\xi_1 - \frac{1}{\tau_1}k_\theta\tilde\theta.\end{aligned} \tag{19}$$

Substituting (19) into the first equation of (18), the position tracking error dynamics becomes

$$\begin{aligned}\dot{\tilde\theta} &= \xi_1 + \tilde\omega,\\ \dot\xi_1 &= -\frac{1}{\tau_1}\xi_1 - \frac{1}{\tau_1}k_\theta\tilde\theta,\end{aligned} \tag{20}$$

where $k_\theta > 0$ is the position controller gain and τ_1 is the time constant of the auxiliary first order position filter.

From the second equation in (18) the speed controller is designed as

$$\begin{aligned}i_q^* &= \frac{1}{\mu\psi^*}(\dot\omega^* + v\omega^* + \widehat T_\mathrm{L} + \xi_2),\\ \dot{\widehat T}_\mathrm{L} &= -k_{\omega i}\tilde\omega,\\ \dot\xi_2 &= -\frac{1}{\tau_2}\xi_2 - \frac{1}{\tau_2}k_\omega\tilde\omega,\end{aligned} \tag{21}$$

where $\widehat T_\mathrm{L}$ is the estimate of $\frac{T_\mathrm{L}}{J}$, load estimation error is defined as $\widetilde T_\mathrm{L} = \frac{T_\mathrm{L}}{J} - \widehat T_\mathrm{L}$, τ_2 is the time constant of the speed filter and $\dot\omega^*$ in (21) is computed from the position controller equation (19) as

$$\dot\omega^* = \ddot\theta^* - \frac{1}{\tau_1}(\xi_1 + k_\theta\tilde\theta).$$

Total position–speed error dynamics is given by

$$\begin{aligned}\dot{\tilde\theta} &= \xi_1 + \tilde\omega,\\ \dot\xi_1 &= -\frac{1}{\tau_1}\xi_1 - \frac{1}{\tau_1}k_\theta\tilde\theta,\end{aligned} \tag{22}$$

$$\begin{aligned}\dot{\widetilde T}_\mathrm{L} &= k_{\omega i}\tilde\omega,\\ \dot{\tilde\omega} &= -v\tilde\omega - \widetilde T_\mathrm{L} + \xi_2 + \frac{\widetilde T}{J},\\ \dot\xi_2 &= -\frac{1}{\tau_2}\xi_2 - \frac{1}{\tau_2}k_\omega\tilde\omega.\end{aligned} \tag{23}$$

Position control loop dynamics (22) is linear and asymptotically stable for $\forall(k_\theta,\tau_1) > 0$, while the speed control loop dynamics (23) can be designed using the three tuning parameters of the speed controller: proportional k_ω and integral $k_{\omega i}$ gains and filter time constant τ_2. Both time constants τ_1 and τ_2 can be selected arbitrarily small. Note that the first order speed and position filters are designed to guarantee a smooth torque (current) reference with known time derivative in (21).

The composite error dynamics is given by (22), (23), (17) and (10). It can be presented in the form of general nonlinear feedback interconnection of the mechanical (22) and (23) and electrical (10) subsystems as

$$\dot{\mathbf{x}}_\mathrm{m} = \mathbf{A}_{\mathrm{m}1}\mathbf{x}_\mathrm{m} + \mathbf{A}_{\mathrm{m}2}(\mathbf{x}_\mathrm{e})\mathbf{x}_\mathrm{m} + \mathbf{B}_1(t)\mathbf{x}_\mathrm{e} + \mathbf{B}_2(\mathbf{x}_\mathrm{e})\mathbf{x}_\mathrm{e}, \tag{24}$$

$$\dot{\mathbf{x}}_\mathrm{e} = \mathbf{A}_\mathrm{e}(\mathbf{x}_\mathrm{m}, t)\mathbf{x}_\mathrm{e}, \tag{25}$$

where $\mathbf{x}_\mathrm{m} = (\tilde\theta, \xi_1, \widetilde T_\mathrm{L}, \tilde\omega, \xi_2)^\mathrm{T}$, $\mathbf{A}_{\mathrm{m}1}$ is a constant Hurwitz matrix given in (22) and (23) with $\widetilde T = 0$, $\mathbf{A}_\mathrm{e}(t)$ in (10) is indicated as $\mathbf{A}_\mathrm{e}(\mathbf{x}_\mathrm{m}, t)$ to enlighten the dependence of ω, ω_0, ω_2 on mechanical error variables $\mathbf{x}_\mathrm{m}$ and time t, and

$$\begin{aligned}\mathbf{A}_{\mathrm{m}2}(\mathbf{x}_\mathrm{e})\mathbf{x}_\mathrm{m} = \Bigg[0,0,0,\frac{\tilde\psi_d}{\psi^*}\Bigg(-\frac{1}{\tau_1}[(1-\tau_1 v)\xi_1 + k_\theta\tilde\theta]\\ -\widetilde T_\mathrm{L} + \xi_2\Bigg),0\Bigg]^\mathrm{T}\end{aligned} \tag{26}$$

$$\begin{aligned}\mathbf{B}_1(t)\mathbf{x}_\mathrm{e} = \Bigg[0,0,0,\left(v\dot\theta^* + \frac{T_\mathrm{L}}{J} + \ddot\theta^*\right)\frac{\tilde\psi_d}{\psi^*} + \mu\psi^*\tilde i_q\\ -\frac{\mu}{\alpha L_\mathrm{m}}(\alpha\psi^* + \dot\psi^*)\tilde\psi_q, 0\Bigg]^\mathrm{T}\end{aligned} \tag{27}$$

$$\mathbf{B}_2(\mathbf{x}_\mathrm{e})\mathbf{x}_\mathrm{e} = \begin{bmatrix}0, & 0, & 0, & \mu(\tilde\psi_d\tilde i_q - \tilde\psi_q\tilde i_d), & 0\end{bmatrix}^\mathrm{T} \tag{28}$$

are obtained from (17), (21) and (8). Main features of system (24) and (25) are

- constant matrix $\mathbf{A}_{\mathrm{m}1}$ is Hurwitz with appropriate tuning of the speed and position controller parameters;
- electrical subsystem (25) is globally exponentially stable;
- interconnection terms given by (26)–(28) have linear/bilinear properties with bounded coefficients under conditions of assumptions A.3 and A.4.

Stability is proved exploiting exponential stability of isolated electromagnetic and mechanical subsystems and special feedback structure of (24) and (25), which has linear/bilinear interconnection properties thanks to torque–flux decoupling. Utilizing the approach reported in [11], it follows that the equilibrium point $(\mathbf{x}_\mathrm{m}^\mathrm{T}, \mathbf{x}_\mathrm{e}^\mathrm{T})^\mathrm{T} = 0$ of the composite system (24) and (25) is globally exponentially stable. Consequently, position tracking control objective CO1 is obtained with all internal signals bounded. Control objectives CO2 and CO3 are achieved since:

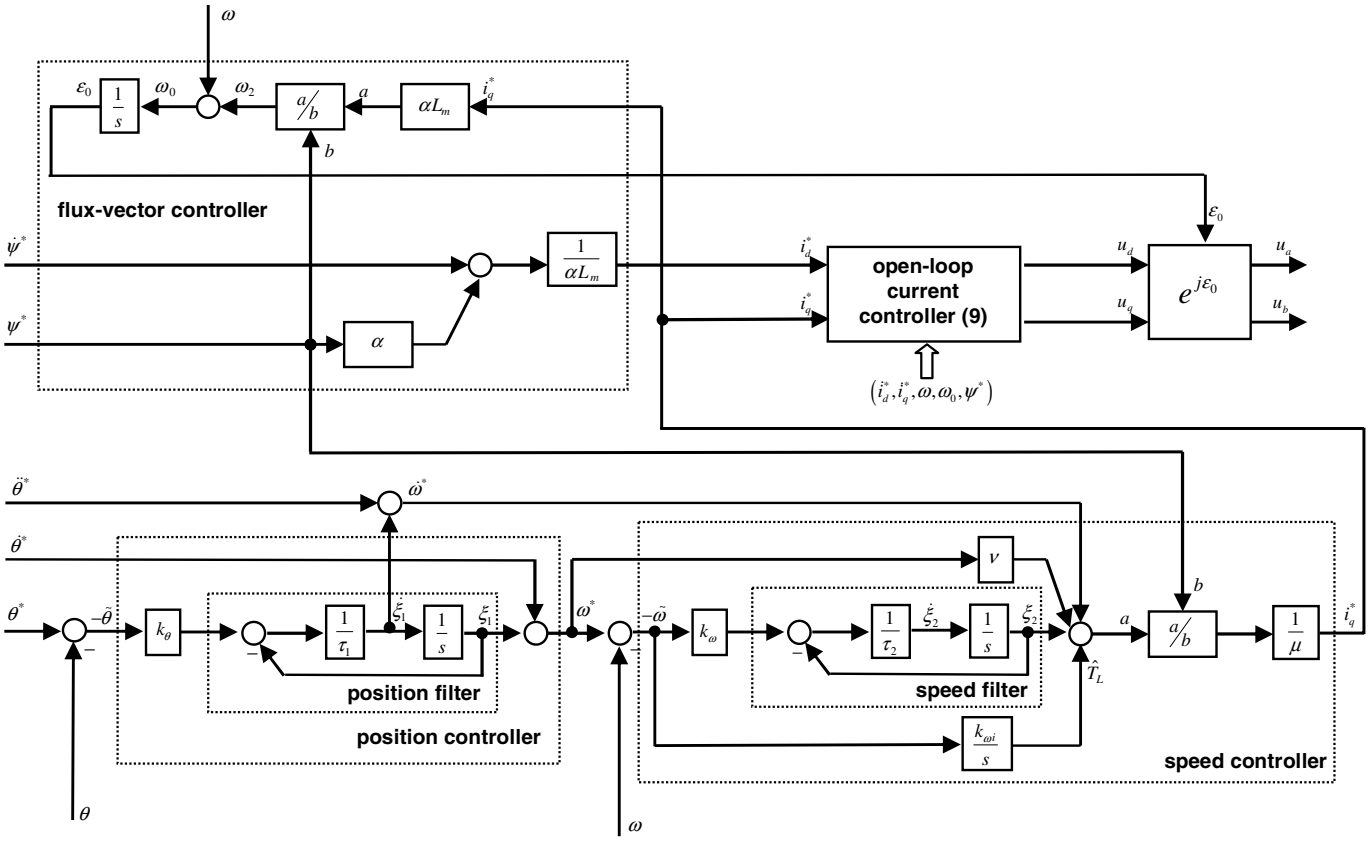


Fig. 1. Block diagram of the position–flux controller proposed.

(a) if $\mathbf{x}_e(0) = 0$, then $\mathbf{x}_e(t) \equiv 0$, $\forall t \geqslant 0$ and the nominal speed/position subsystem $\dot{\mathbf{x}}_m = \mathbf{A}_{m1}\mathbf{x}_m$ is linear and independent of the flux/current control;
(b) if $\mathbf{x}_e(0) \neq 0$, then subsystem (24) can be viewed as the nominal mechanical one perturbed by the exponentially vanishing perturbation generated by subsystem (25).

The block diagram of the controller is reported in Fig. 1.

4. Comparison with the V-type control

In this section the speed–flux tracking controller obtained from (8), (9) and (21), i.e. removing the outer position control loop, is compared with the V-type controller designed in [15], whose equations are recalled here for the sake of clarity

$$\begin{aligned} i_d^* &= \frac{1}{\alpha L_m}(\alpha\psi^* + \dot{\psi}^*), \\ \dot{\varepsilon}_0 &= \omega_0 = \omega + \alpha L_m \frac{i_q^*}{\psi^*}, \end{aligned} \tag{29}$$

$$\begin{aligned} i_q^* &= \frac{1}{\mu\psi^*}(\dot{\omega}^* + \nu\omega^* + \widehat{T}_L - k_\omega\tilde{\omega}), \\ \widehat{T}_L &= -k_{\omega i}\tilde{\omega}, \end{aligned} \tag{30}$$

$$\begin{aligned} u_d &= \sigma(\gamma i_d^* - \omega_0 i_q^* - \alpha\beta\psi^*), \\ u_q &= \sigma(\gamma i_q^* + \omega_0 i_d^* + \beta\omega\psi^*). \end{aligned} \tag{31}$$

In Eqs. (29) and (30) standard IFOC and PI speed control with feed-forward actions are reported, while the V-type control is represented by (31).

Assuming constant flux and speed references ψ^*, ω^* and load torque T_L, from (1) and (29)–(31) the linearized error dynamics of the full-order IM model with the V-type control is

$$\begin{bmatrix} \dot{\tilde{i}}_d \\ \dot{\tilde{i}}_q \\ \dot{\tilde{\psi}}_d \\ \dot{\tilde{\psi}}_q \\ \dot{\tilde{T}}_L \\ \dot{\tilde{\omega}} \end{bmatrix} = \begin{bmatrix} -\gamma & \bar{\omega}_0 & \alpha\beta & \beta\omega^* & 0 & 0 \\ -\bar{\omega}_0 & -(\gamma - k_\omega) & -\beta\omega^* + \dfrac{k_\omega}{\mu\psi^{*2}}\left(\nu\omega^* + \dfrac{T_L}{J}\right) & \alpha\beta - \dfrac{k_\omega}{L_m} & -\dfrac{k_\omega}{\mu\psi^*} & \dfrac{1}{\mu\psi^*}(k_{\omega i} - k_\omega(\nu + k_\omega)) \\ \alpha L_m & 0 & -\alpha & \bar{\omega}_0 - \omega^* & 0 & 0 \\ 0 & \alpha L_m & -(\bar{\omega}_0 - \omega^*) & -\alpha & 0 & 0 \\ 0 & 0 & 0 & 0 & 0 & k_{\omega i} \\ 0 & \mu\psi^* & \dfrac{1}{\psi^*}\left(\nu\omega^* + \dfrac{T_L}{J}\right) & -\dfrac{\mu\psi^*}{L_m} & -1 & -(\nu + k_\omega) \end{bmatrix} \cdot \begin{bmatrix} \tilde{i}_d \\ \tilde{i}_q \\ \tilde{\psi}_d \\ \tilde{\psi}_q \\ \tilde{T}_L \\ \tilde{\omega} \end{bmatrix}, \tag{32}$$

where

$$\bar{\omega}_0 = \omega^* + \frac{\alpha L_m}{\mu \psi^{*2}} \left(v\omega^* + \frac{T_L}{J} \right).$$

From (10) and (23) the linearized error dynamics with the proposed speed–flux controller is given by

$$\begin{bmatrix} \dot{\tilde{i}}_d \\ \dot{\tilde{i}}_q \\ \dot{\tilde{\psi}}_d \\ \dot{\tilde{\psi}}_q \\ \dot{\tilde{T}}_L \\ \dot{\tilde{\omega}} \\ \dot{\xi}_2 \end{bmatrix} = \begin{bmatrix} -\gamma & \bar{\omega}_0 & \alpha\beta & \beta\omega^* & 0 & 0 & 0 \\ -\bar{\omega}_0 & -\gamma & -\beta\omega^* & \alpha\beta & 0 & 0 & 0 \\ \alpha L_m & 0 & -\alpha & \bar{\omega}_0 - \omega^* & 0 & 0 & 0 \\ 0 & \alpha L_m & -(\bar{\omega}_0 - \omega^*) & -\alpha & 0 & 0 & 0 \\ 0 & 0 & 0 & 0 & 0 & k_{\omega i} & 0 \\ 0 & \mu\psi^* & \frac{1}{\psi^*}\left(v\omega^* + \frac{T_L}{J} \right) & -\frac{\mu\psi^*}{L_m} & -1 & -v & 1 \\ 0 & 0 & 0 & 0 & 0 & -\frac{1}{\tau_2} k_\omega & -\frac{1}{\tau_2} \end{bmatrix} \cdot \begin{bmatrix} \tilde{i}_d \\ \tilde{i}_q \\ \tilde{\psi}_d \\ \tilde{\psi}_q \\ \tilde{T}_L \\ \tilde{\omega} \\ \xi_2 \end{bmatrix}. \quad (33)$$

From (33) it follows that with the proposed controller the electromagnetic subsystem is coupled in series interconnection with the mechanical subsystem. On the contrary, from the structure of system matrix in (32) it results that with the V-type control the electromagnetic and speed error dynamics are feedback interconnected subsystems, due to the uncompensated tracking error-dependent terms in the expression of $\dot{i}_q^*$. This fact is particularly important since the interconnection terms between the speed and flux subsystems depend on gains k_ω, $k_{\omega i}$ and the current error dynamics cannot be set arbitrarily fast due to the absence of current feedback control.

In Fig. 2 position of eigenvalues of matrices in (32) and (33) are comparatively shown as a function of k_ω. Speed proportional gain k_ω varies in the range [20, 300], while other control parameters have been set as $k_{\omega i} = k_\omega^2/2$, $\tau_2 = 0.001$. The IM parameters adopted for this study are reported in the Appendix. In Fig. 2a it can be noted that with the proposed controller the eigenvalues of the electromagnetic subsystem are independent of k_ω (they are Hurwitz and depend on the operating conditions through ω^*, ψ^*, T_L, see also considerations in Section 3.1), while eigenvalues of the mechanical part are well damped (see also Section 3.2). In Fig. 2b it is shown that, with the V-type control, coupling terms lead to poorly damped or even unstable eigenvalues for high values of k_ω.

Simulation tests have been performed in order to compare the dynamic performance of the proposed speed controller with the V-type controller. Controller parameters are selected as $k_\omega = 160$, $k_{\omega i} = 12{,}800$, $\tau_2 = 0.001$. In Fig. 3 the speed and flux references and the load torque

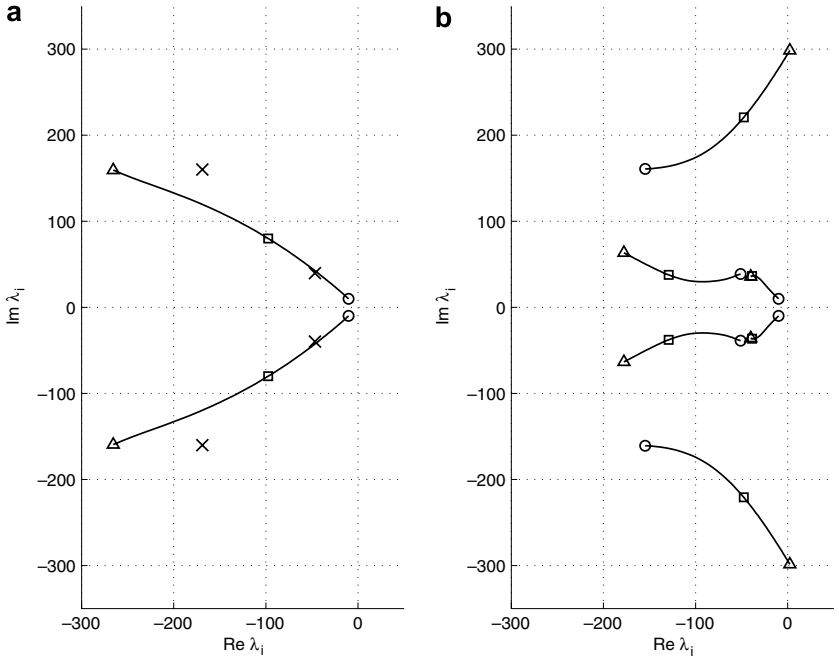


Fig. 2. Root loci of the linearized error models, for $\omega^* = 100$ rad/s, $\psi^* = 0.86$ Wb/s, $T_L = 0$ N m. (a) Position of the dominant eigenvalues with the proposed controller, for $k_\omega \in [20, 300]$: eigenvalues of the electromagnetic part are indicated with ×, eigenvalues of the mechanical part with ○ for $k_\omega = 20$, with □ for $k_\omega = 160$ and with △ for $k_\omega = 300$. (b) Position of the eigenvalues with the V-type controller, for $k_\omega \in [20, 300]$: eigenvalues are indicated with ○ for $k_\omega = 20$, with □ for $k_\omega = 160$ and with △ for $k_\omega = 300$.

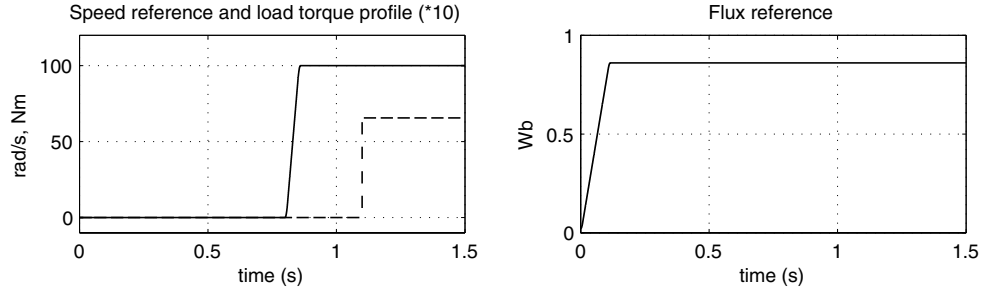


Fig. 3. Speed and flux references and load torque profile of the simulation tests.

profile during simulation are depicted. The operating sequences are the following. After the initial flux excitation phase from $t = 0$ to $t = 0.11$ s with $\psi^*(0) = 0.02$ Wb, a constant rated flux reference $\psi^* = 0.86$ Wb is imposed. From 0.8 s to 0.86 s the speed reference goes from zero to 100 rad/s with rated motor torque (7.0 N m) required during speed transient. At $t = 1.1$ s constant rated load torque (7.0 N m) is applied.

Simulation results reported in Figs. 4 and 5 confirm the analysis based on the linearized dynamics. In particular, in Fig. 4 the dynamic behaviour of the proposed speed controller is shown. Well damped speed response is obtained

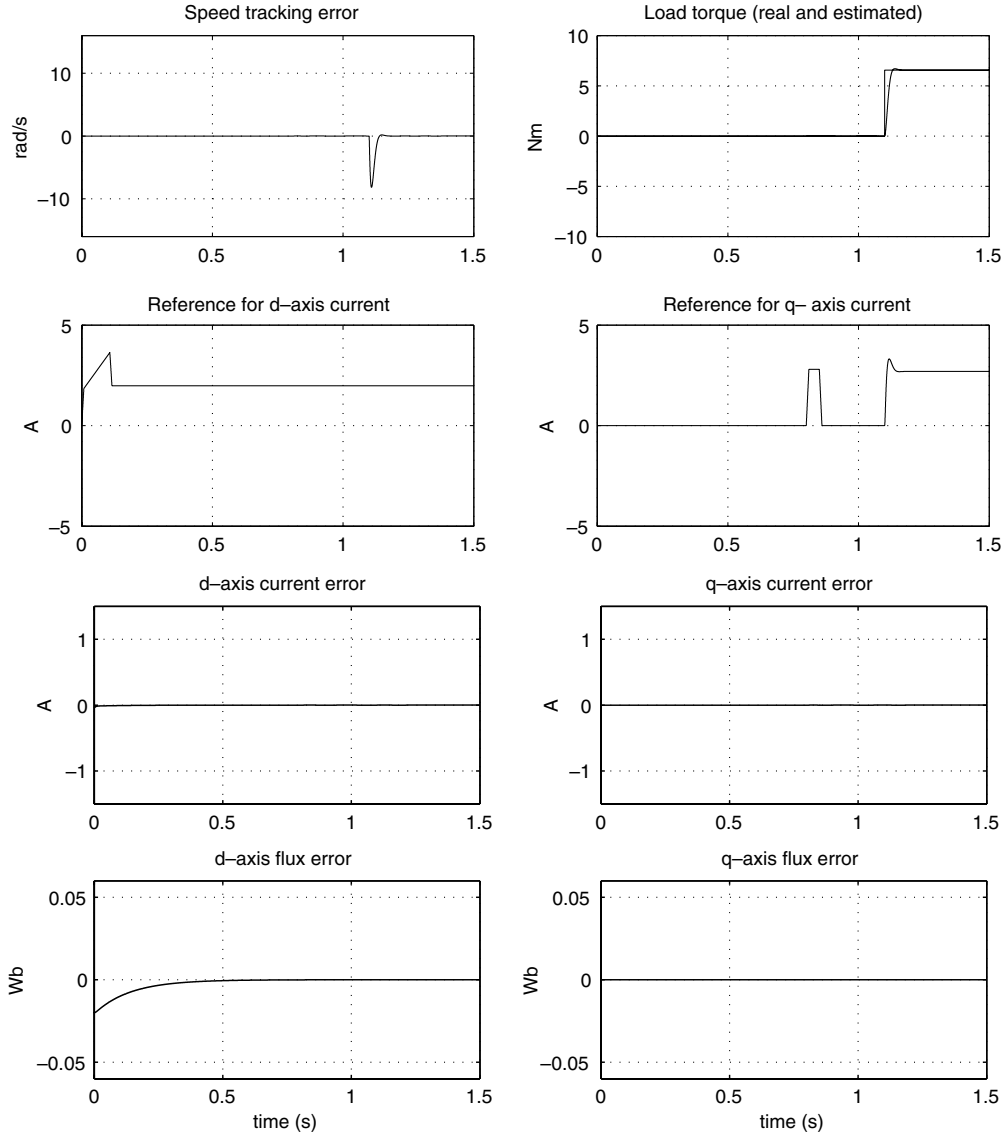


Fig. 4. Simulation results. Dynamic behaviour of the proposed speed controller.

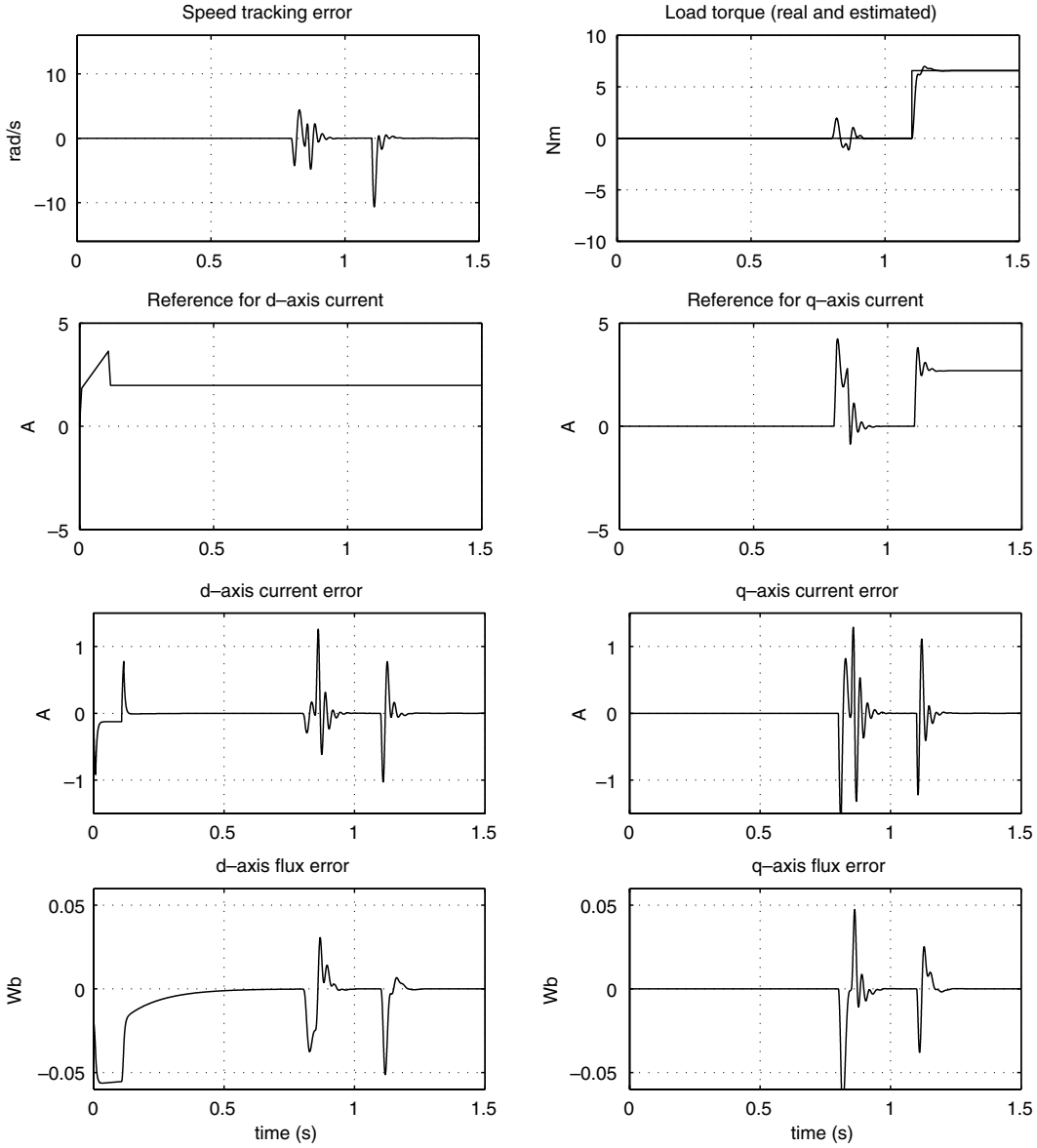


Fig. 5. Simulation results. Dynamic behaviour of the V-type controller.

during constant rated load torque rejection, and perfect tracking of speed reference is guaranteed, thanks to decoupling of mechanical and electrical IM subsystems. Flux and current errors tend exponentially to zero and are not perturbed during speed transient.

In Fig. 5 the behaviour of the V-type controller is depicted. Due to interconnection between electrical and mechanical subsystems, flux and current errors are present during speed transient and load torque rejection phases, and oscillatory speed response is obtained. Note that large flux error is present during the initial phase due to absence of dynamic feed-forward terms in the d-axis voltage.

From these considerations it comes out that in order to prevent poorly damped responses or even instability, gains k_ω, $k_{\omega i}$ (and hence the speed controller bandwidth) must be limited with the V-type control. Thanks to torque–flux decoupling, the proposed controller ensures better dynamic performances with respect to the V-type control.

5. Experimental results

Experimental tests have been carried out using a 1.1 kW standard induction motor in order to evaluate the performance of the proposed control algorithm.

5.1. Operating sequences

Flux and position reference trajectories are presented in Fig. 6 using solid lines; dashed line in the same figure represents the load torque profile. The operating sequences of the experiments are the following:

1. The machine is excited during the initial time interval 0–0.11 s imposing a flux reference trajectory starting at $\psi^*(0) = 0.02$ Wb and reaching the motor rated value of 0.86 Wb with the first and second derivatives equal to 8 Wb/s and 1000 Wb/s^2 correspondingly.

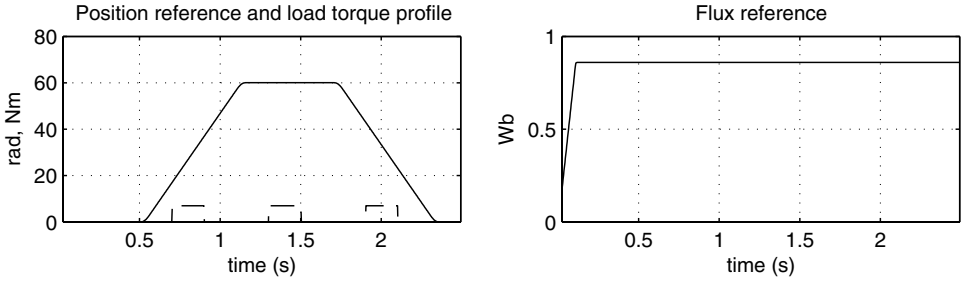


Fig. 6. Experimental tests. Position, flux references and load torque profile.

2. The motor is required to track the position reference trajectory, characterized by the following phases: starting at $t = 0.5$ s from zero initial value, the position reference reaches the value of 60 rad at $t = 1.15$ s; from $t = 1.15$ s to $t = 1.7$ s the position reference is maintained constant, and from $t = 1.7$ s to $t = 2.35$ s the motor is required to come back to 0 rad. Maximum absolute values of the speed reference and of its first and second derivatives are equal to 100 rad/s, 2000 rad/s^2, 2×10^5 rad/s^3 correspondingly. Tracking of the position reference trajectory adopted requires a torque equal to the motor rated value.
3. From time $t = 0.7$ s to $t = 0.9$ s, from $t = 1.3$ s to $t = 1.5$ s and from $t = 1.9$ s to $t = 2.1$ s a constant load torque, equal to 100% of the motor rated value (7.0 N m), is applied. During other time intervals load torque is set to zero.

5.2. Controller parameters

Referring to (22) and (23) the controller parameters can be grouped into two sets: position and speed controller gains k_θ, k_ω, $k_{\omega i}$ and time constants τ_1, τ_2.

Considering the ideal case of $\tau_1 = \tau_2 = 0$, the mechanical error dynamics is composed by the 1st order position dynamics cascaded with the second order speed dynamics. The position controller gain k_θ is set in order to impose the bandwidth of the position control loop. The parameters of the speed subsystem k_ω, $k_{\omega i}$ are tuned accordingly to standard tuning relations

$$\frac{1}{\tau^2} = k_{\omega i} \quad \text{and} \quad k_{\omega i} = \left(\frac{k_\omega^2}{2}\right) \ (\delta = 0.707) \quad \text{or}$$

$$k_{\omega i} = \left(\frac{k_\omega}{2}\right)^2 \ (\delta = 1),$$

where τ and δ are time constant and damping factor of the second order speed error subsystem. Following common tuning procedure for cascaded control architectures, speed controller bandwidth is set sensibly larger than the position controller one. Time constants τ_1, τ_2 are set sufficiently small in order to be negligible with respect to the dynamics of the speed and position control loops.

In the experiments, the controller tuning parameters are set as follows:

$k_\theta = 60, \quad k_\omega = 160, \quad k_{\omega i} = 12,800, \quad \tau_1 = 0.001$ s, $\tau_2 = 0.001$ s.

5.3. Experimental set-up

The experimental tests were carried out at L.A.R. (Automation and Robotics Laboratory) of the University of Bolo-

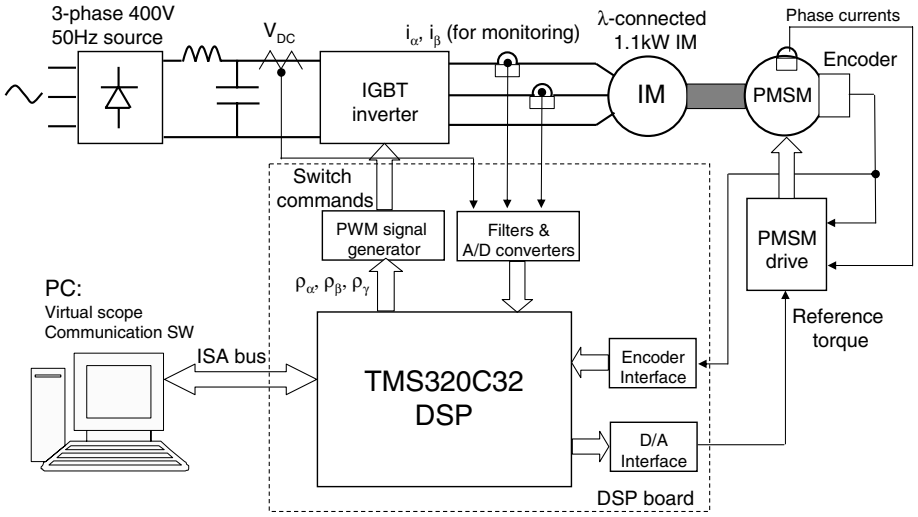


Fig. 7. Block diagram of the Rapid Prototyping Station.

gna, using a rapid prototyping station (RPS), whose schematic block diagram is shown in Fig. 7. The RPS includes:

1. A Personal Computer acting as the Operator Interface during the experiments.
2. A custom floating-point digital signal processor (DSP) board (based on TMS320C32) directly connected to the PC bus. The DSP board performs data acquisition (eight 12-bit A/D data channels plus two interfaces for incremental encoder), implements control algorithms and generates the PWM signals (two symmetrical three-phase PWM modulators with programmable dead time).
3. A 50 A/380 V_{RMS} three-phase inverter, operated at 10 kHz switching frequency. Dead time has been set to

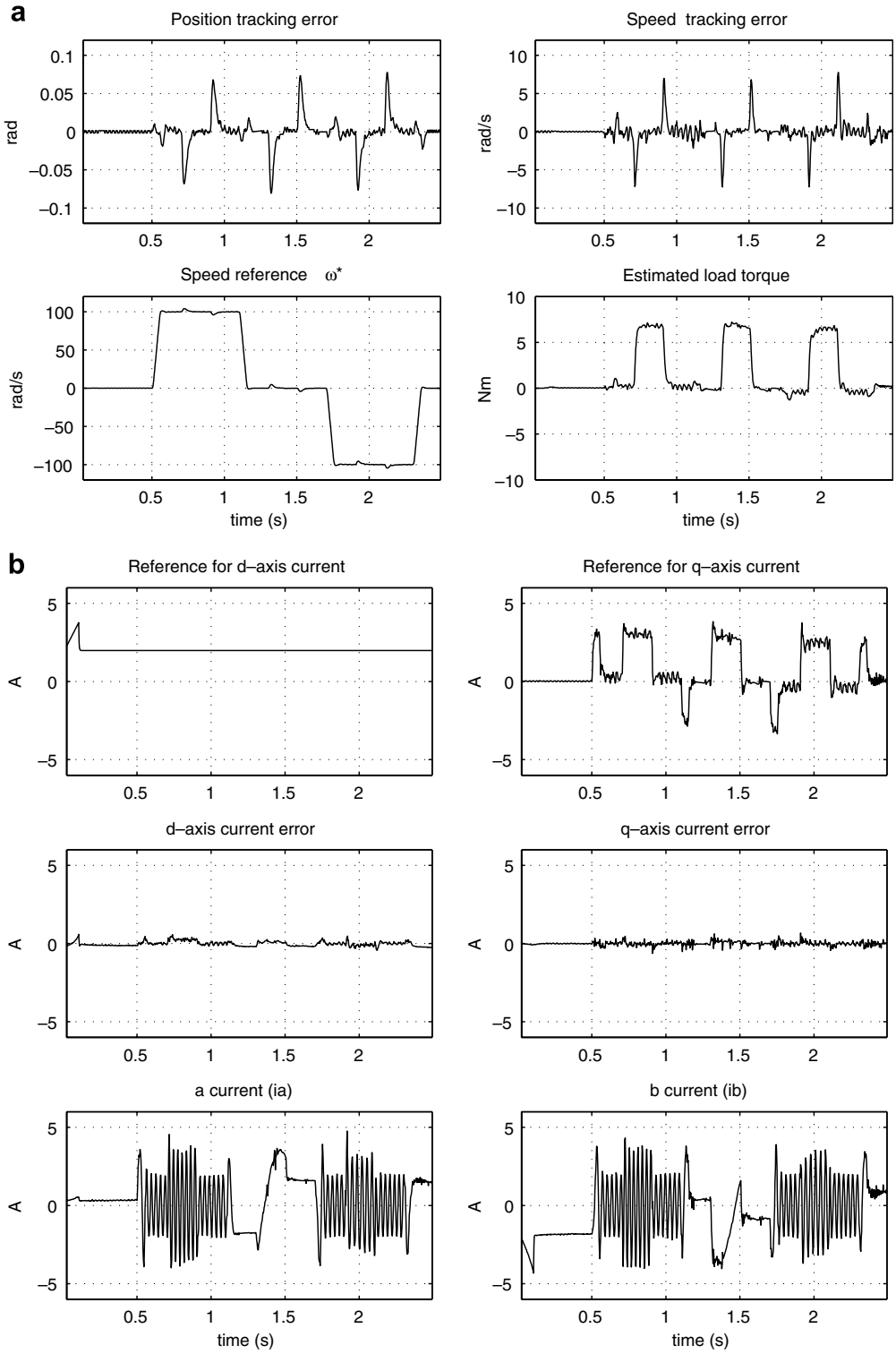


Fig. 8. Dynamic behaviour of the position controller with nominal IM parameters: (a) mechanical variables; (b) stator currents; (c) stator voltages.

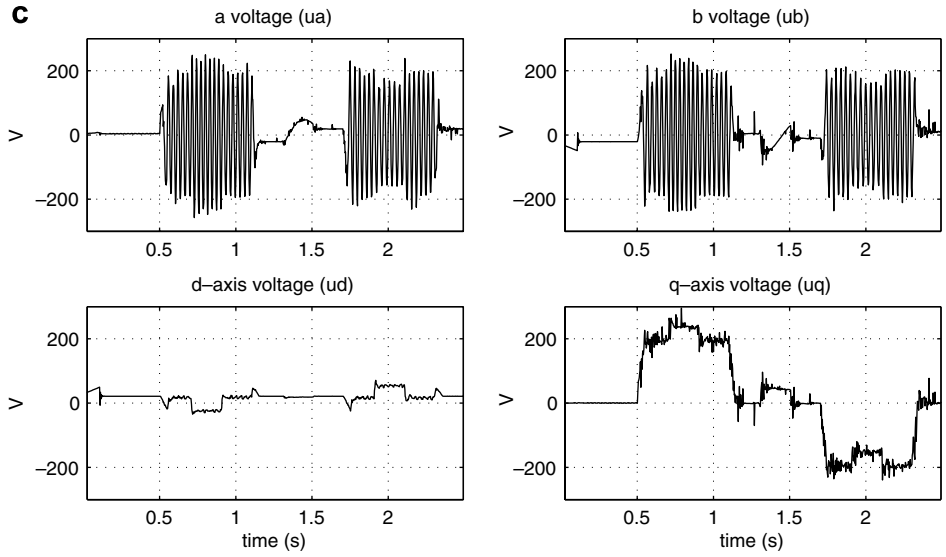


Fig. 8 (*continued*)

1.5 μs. It is worth noting that a 50 A inverter has been adopted since it is part of the RPS available at L.A.R.; current required in the experiments is much lower and consistent with the size of the adopted induction motor, the overall inertia, the required dynamic performances and the load torque.

4. A 4-pole, 50 Hz, 1.1 kW induction servomotor, whose data are listed in the Appendix.
5. A vector-controlled permanent magnet synchronous motor used to provide the load torque.

5.4. Measurement system and controller implementation

The motor position and speed are measured by means of a 512 pulse/revolution incremental encoder. Two stator phase currents are measured only for monitoring purposes, by means of Hall-effect zero-field sensors, simultaneously and synchronously sampled at the symmetry point of the PWM signals. The sampling time for the controller is set to 200 μs. In order to get the discrete-time version of the control algorithm the simple Euler method is used. Inverter dead time effect (1.5 μs) has not been compensated in the control algorithm. The computational time required for the algorithm implementation is 40 μs with the utilized DSP.

5.5. Experimental results

A first set of experimental results, reported in Fig. 8a–c, has been performed in order to test the dynamic behaviour of the control algorithm during position trajectory tracking and load torque rejection. The transient performance is characterized by a maximum position error of about 0.02 rad during reference trajectory tracking and about 0.07 rad during rejection of step-wise changing of the load torque. During phases with constant speed reference and constant load torque, the steady-state position tracking error is zero. Maximum speed error $\tilde{\omega}$ is about 2 rad/s during reference trajectory tracking and about 7 rad/s during constant load torque rejection. A settling time of about 80 ms during step load torque rejection is obtained. Similar performances during rejection of constant load torque are obtained in the high-speed/load-torque case ($t \in [0.7, 0.9]$ s), in the high-speed/regenerative-torque case ($t \in [1.9, 2.1]$ s) and at zero speed ($t \in [1.3, 1.5]$ s). Correct estimation of the load torque is obtained by means of the integral action of the PI speed controller as $J \cdot \widehat{T}_{\mathrm{L}}$. Negligible current regulation errors are present during the experiments proving that the achievable tracking performance is the same as in the case of vector IM drives with current feedback control. Effects of plant non-idealities, such as inverter dead time and voltage actuation distortion, are relevant only at low and zero speed, when applied stator voltage is low. Stator currents and voltages in the (a–b) reference frame are reported, too.

A second set of experiments has been performed with the parameter $\hat{\alpha} = \hat{R}_{\mathrm{r}}/\hat{L}_{\mathrm{r}}$ (inverse of rotor time constant), used in the control algorithm, different from the actual one, α_N. Figs. 9 and 10 demonstrate the transients obtained for $\hat{\alpha} = 20\ \mathrm{s}^{-1}$ ($2.0\alpha_N$) and $\hat{\alpha} = 6\ \mathrm{s}^{-1}$ ($0.6\alpha_N$), with the same position–flux reference and load torque profile of the first experiment. Non-null steady-state current tracking error is present when motor torque is required, due to error on α. On the other hand, it can be noted that the actual i_d and i_q currents are close to the nominal case during steady-state conditions, enlightening good flux orientation. This behaviour mainly depends on the absence of current feedback control and can be explained recalling the physical considerations reported in [15]. During transients, maximum position and speed tracking errors are 9 rad and 9 rad/s correspondingly. This dynamic performance degradation (about 25% with respect to the nominal case) is due to the spurious torque–flux coupling induced by the wrong control parameter $\hat{\alpha}$ during speed/torque transients.

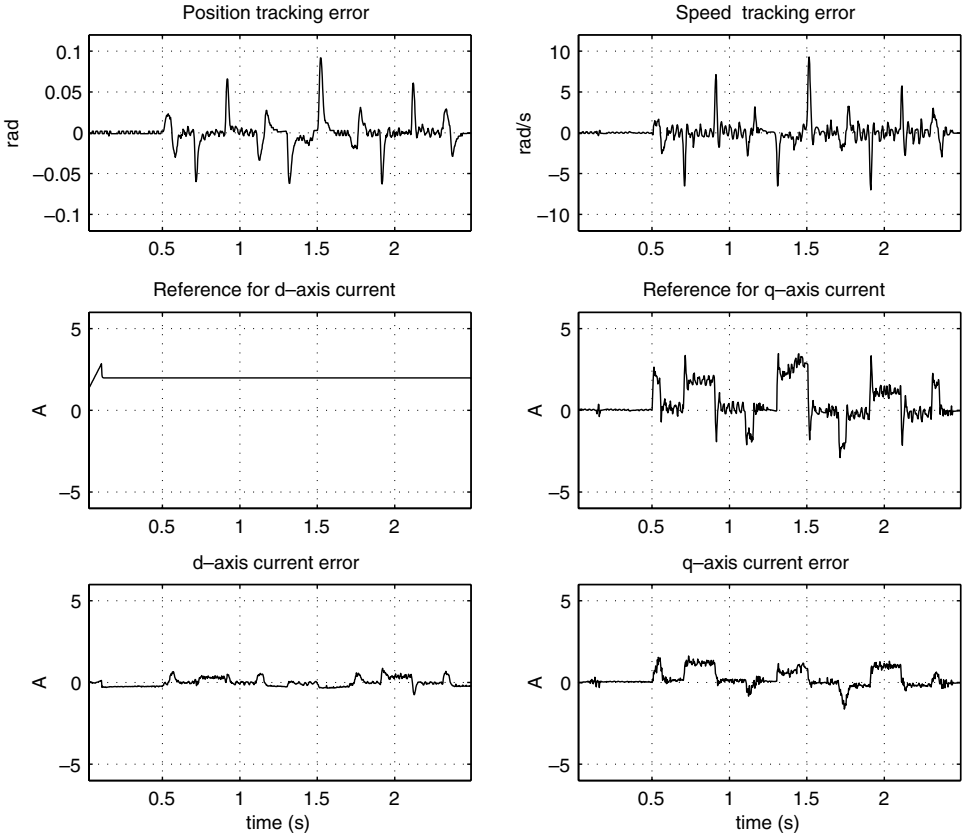


Fig. 9. Dynamic behaviour of the position controller with $\hat{\alpha}$ equal to $2.0\alpha_N$.

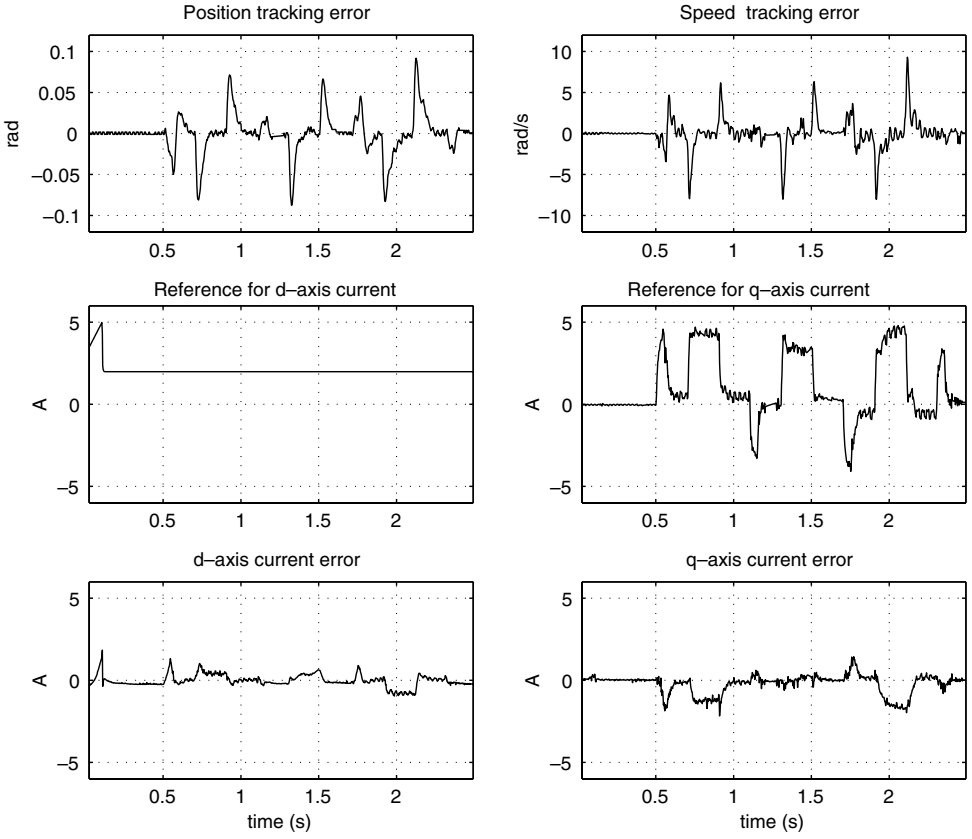


Fig. 10. Dynamic behaviour of the position controller with $\hat{\alpha}$ equal to $0.6\alpha_N$.

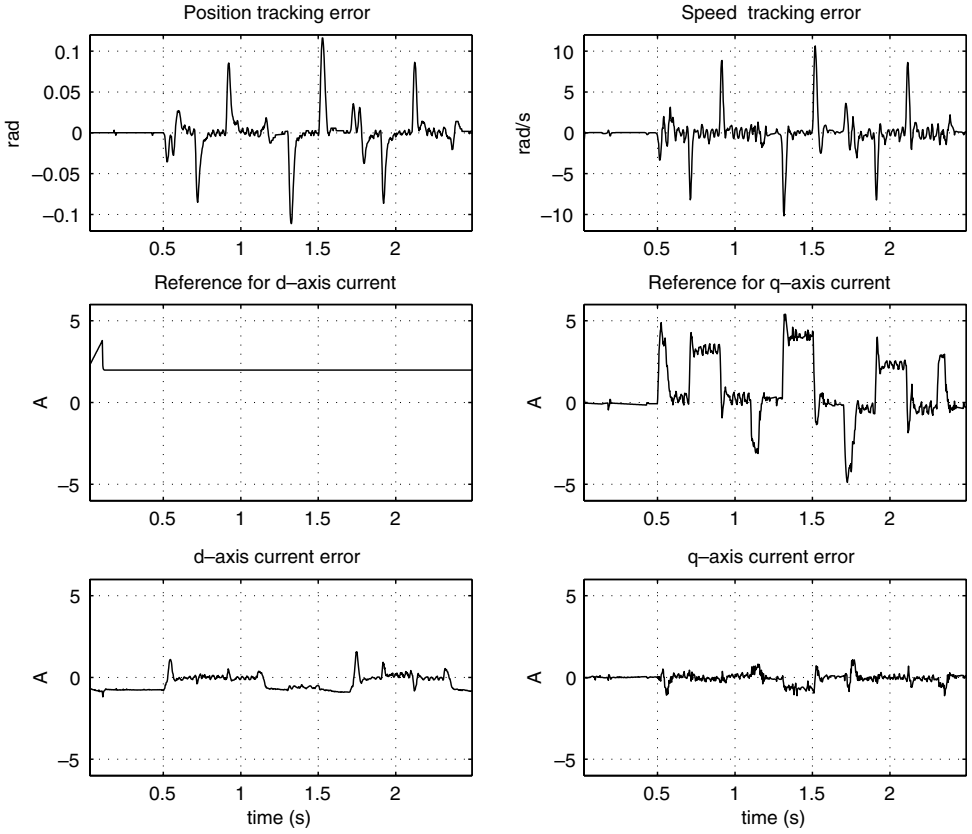


Fig. 11. Dynamic behaviour of the position controller with $\hat{R}_s$ equal to $0.7R_{sN}$.

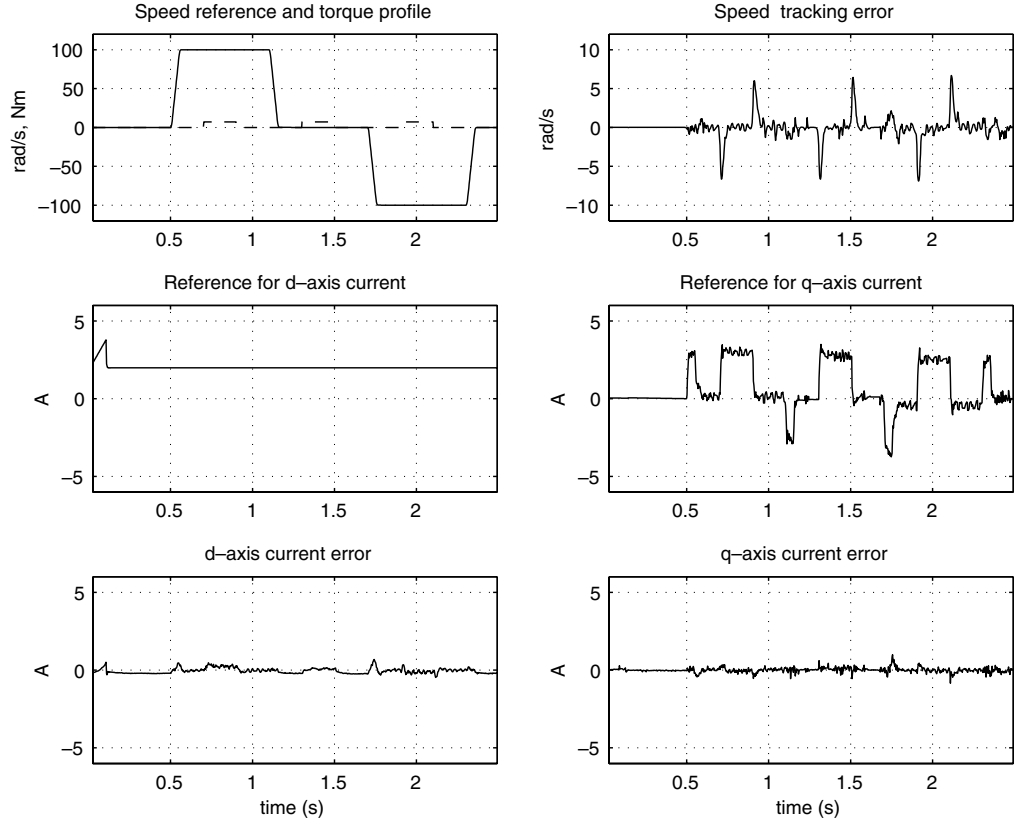


Fig. 12. Dynamic behaviour of the speed controller with nominal IM parameters.

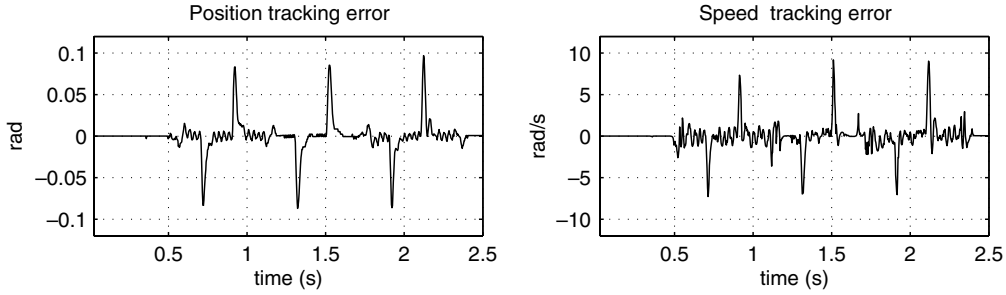


Fig. 13. Dynamic behaviour of the position controller with nominal IM parameters and sampling time equal to $T_s = 600$ μs.

A third set of experiments has been made with imperfect knowledge of the stator resistance. The transient obtained for $\hat{R}_s = 0.7R_{sN}$ (where $\hat{R}_s$ is the value adopted in the control algorithm, while R_{sN} is the actual one), is shown in Fig. 11. Despite of the non-null steady-state regulation error present on the flux current i_d, mostly at zero speed, maximum position tracking error is 11 rad during constant load torque rejection at zero speed, while no performance degradation is enlightened during other operating conditions. The experimental tests demonstrate that the proposed controller shows good robustness properties with respect to rotor time constant and stator resistance variations.

The current sensorless speed–flux controller obtained from (8), (9) and (21), i.e. removing the outer position controller loop, has been experimentally tested. In this experiment, the IM is required to track the speed reference obtained differentiating the position reference of Fig. 6, while flux reference and load torque profile are the same of Fig. 6. In Fig. 12 the results are reported. Maximum speed tracking error is 6 rad/s during constant rated load torque rejection, while the speed tracking error is negligible during speed transients. A settling time of about 60 ms during step load torque rejection is obtained.

The position controller has been tested also with a sampling time equal to $T_s = 600$ μs in order to check performances when low cost and computational power control devices are utilized. Selected gain for the position and speed controller are the same used for the tests with $T_s = 200$ μs, while time constants of the auxiliary filters are set to $\tau_1 = \tau_2 = 0.0015$ s. In Fig. 13 the dynamic behaviour of the position controller is shown, under the same operating conditions of previous tests, utilizing the nominal parameters in the controller. Comparison of Figs. 8 and 13 shows a performance degradation of not more than 20%, considering the maximum position tracking error during transient conditions.

Finally, from the presented tests it can be noted that in any working condition, even with significant parameter errors, the actual currents are not significantly far from their references, which are always consistent with the IM size. Hence, no oversizing of the inverter is necessary when the proposed control algorithm is adopted.

6. Conclusions

A new stator current sensorless position–flux tracking control algorithm is presented. It is based on concept of natural indirect field-orientation and provides global asymptotic position and rotor flux modulus tracking in presence of constant unknown load torque. Asymptotic decoupling of the mechanical and electrical error variables together with asymptotic field orientation are achieved, leading to robust cascaded structure of the speed and position control loops connected in series with the IM electrical subsystem. Experimental results demonstrate good robustness properties with respect to electrical motor parameter variations and prove that the achievable position (speed) tracking performances are suitable for a wide spectrum of low cost servo applications.

Appendix.

Nominal parameters of the induction motor adopted for the experimental test

Induction motor data:	
Rated power	1.1 kW
Rated speed	1500 rev/min
Rated torque	7.0 N m
Rated frequency	50 Hz
Pole pairs	2
Excitation current	1.4 A
Rated current	2.8 A
Stator resistance	10.2 Ω
Rotor resistance	4.8 Ω
Magnetization inductance	0.434 H
Stator inductance	0.48 H
Rotor inductance	0.46 H
Total inertia	0.0034 kg m^2

References

[1] Leohnard W. Control of electric drives. Berlin, Germany: Springer-Verlag; 1995.
[2] Novotny DW, Lipo TA. Vector control and dynamics of AC drives. Oxford, UK: Oxford University Press; 1996.

[3] Lorenz RD. Advances in electric drive control. In: International conference on electric machines and drives IEMD 1999; 9–12 May 1999. p. 9–16.
[4] Blaschke F. The principle of field orientation applied to the new transvector closed-loop control system for rotating field machines. Siemens-Rev 1972;39:217–20.
[5] Kim D, Ha I, Ko M. Control of induction motors via feedback linearization with input–output decoupling. Int J Control 1990;51(4):863–83.
[6] Ortega R, Nicklasson PJ, Espinosa G. On speed control of induction motors. Automatica 1996;32(3):455–60.
[7] Nicklasson PJ, Ortega R, Espinosa G. Passivity-based control of a class of Blondell–Park transformable electric machines. IEEE Trans Automat Control 1997;42(5):629–47.
[8] Kanellakopoulos I, Krein P, Disilvestro F. Nonlinear flux-observer based control of induction motor. In: Proc. American Control Conf. 1992, Chicago, IL, USA; 1992.
[9] Hu J, Dawson DM, Vedagarbha P. A singularity free position tracking controller for induction motors: theory and experiments. In: Proc. 4th IEEE Conf. on Control Application, USA, 1995. p. 985–90.
[10] Khalil HK, Strangas EG. Robust speed control of induction motors using position and current measurements. IEEE Trans Automat Control 1996;41(8):1216–20.
[11] Peresada S, Tonielli A. High performance robust speed–flux tracking controller for induction motor. Int J Adapt Control Signal Process 2000;14(2):177–200.
[12] Peresada S, Tilli A, Tonielli A. Theoretical and experimental comparison of indirect field-oriented controllers for induction motors. IEEE Trans Power Electron 2003;18(1):151–63.
[13] Ohnishi K, Suzuki H, Miyachi K, Terashima M. Decoupling control of flux and secondary current in induction motor drive with controlled voltage source and its comparison with Volts/Hertz control. IEEE Trans Ind Appl 1985;21(Jan./Feb.).
[14] Palma JP, Dente JG. Induction motor drive positioning with a simplified vector control strategy. In: Proc. 7th IEEE Mediterranean electrotechnical conference, 12–14 April 1994. vol. 2. p. 785–8.
[15] Harashima F, Kondo S, Ohnishi K, Kajita M, Susono M. Multimicroprocessor-based control system for quick response induction motor drive. IEEE Trans Ind Appl 1985;IA-21(4).
[16] Asher GM, Summer M. Parallelism and the transputer for real-time high-performance control of AC induction motors. IEE Proc 1990;137(Part D, no. 4).
[17] Feemster M, Vadagarbha P, Haste D, Dawson DM. Adaptive output-feedback control of induction motors. In: Proc. 36th IEEE decision and control conference CDC97, 10–12 December 1997. vol. 2. p. 1950–1955.
[18] Diamantidis D, Krishnan R, Lee S. Design and development of a low cost inverter drive for induction motors. In: Proc. 11th IEEE applied power electronics conference and exposition, APEC '96, 3–7 March 1996. vol. 2. p. 771–7.